Optimization of the Dick effect in an optical lattice clock

Philip G. Westergaard, Jérôme Lodewyck and Pierre Lemonde LNE-SYRTE, Observatoire de Paris, CNRS, UPMC
61 avenue de l'Observatoire, 75014 Paris, France

***Abstract*— We discuss the optimization of the Dick effect in an optical lattice clock. We show that optimizing the time sequence of operation of the clock can lead to a significant reduction of the clock stability degradation by the frequency noise of the interrogation laser. By using a non-destructive detection of the atoms, we are able to recycle most of the atoms between cycles and consequently to strongly reduce the time spent capturing the atoms in each cycle. With optimized parameters, we expect a fractional Allan deviation better than $2 \cdot 10^{-16}\,\tau^{-1/2}$ for the lattice clock.**

I. Introduction

Combined with a superb frequency accuracy, superior ultimate stabilities have been advocated as appealing advantages of optical lattice clocks [1]. In such devices, optical resonances with linewidth down to 2 Hz have been observed [2]. For a typical atom number of 10^5 the corresponding standard quantum limit of the clock Allan deviation lies below $10^{-17}\,\tau^{-1/2}$ with τ being the averaging time in seconds. While vast improvements have been performed over the last few years [3]–[6], the stability of actual lattice clocks is presently more than two orders of magnitude above this "Holy Grail". One stumbles upon the Dick effect, by which the probe laser frequency noise is converted down to low Fourier frequencies by the sampling process inherent to the clock's cyclic operation [7]–[9]. A strenuous effort is presently going on to further reduce the noise of ultra-stable laser sources [10]–[14] but quite hard limitations like the thermal noise of high finesse Fabry-Pérot cavities limit progress in that direction [15]. Comparatively little effort has been put so far on the optimization of the time sequence for the operation of lattice clocks for reducing the Dick effect. We show here that following this direction can lead to very significant improvements.

A key parameter for the Dick effect is the dead time of the clock cycle, during which atoms are prepared (captured, cooled, optically pumped) and detected and do not experience the probe laser frequency noise. This loss of information leads to the frequency stability degradation. In order to dwarf the dead time of the experiment, we propose to keep the atoms from one clock cycle to the next which is made possible by a non-destructive measurement scheme [16]. We discuss here in detail the potential gain in terms of frequency stability that can be achieved using this detection scheme.

In section II, we give a quantitative discussion of the Dick effect in the limit where the dead time approaches 0. We show that for dead times below 100 ms, the limitation of the Allan deviation due to the Dick effect can be reduced to below $10^{-16}\,\tau^{-1/2}$ using Ramsey spectroscopy and state-of-the-art ultra-stable lasers. In section III the new non-destructive detection scheme is described. Finally, section IV discusses the optimization of a Sr lattice clock sequence using the non-destructive scheme, and gives an estimate on the expected stability of the clock.

II. The Dick Effect in the low dead time limit

In a sequentially operated atomic clock, the response of the atoms to the interrogation oscillator frequency fluctuations $\delta\omega(t)$ is dictated by the sensitivity function $g(t)$. The change in transition probability δP due to frequency noise is given by

$$\delta P = \frac{1}{2}\int g(t)\delta\omega(t)dt, \tag{1}$$

where the integral is taken over one clock cycle. The appearance of $g(t)$ depends on the type of interrogation used. In an optical lattice clock either Rabi or Ramsey interrogation can be used. We call T_i the duration of the interrogation π-pulse in the Rabi case and τ_p the duration of each of the two $\pi/2$-pulses and T the free evolution time in the Ramsey case. If T_d is the dead time used to prepare and detect atoms, we define the duty cycle $d = \frac{T_i}{T_c}$ (Rabi) and $d = \frac{2\tau_p+T}{T_c}$ (Ramsey) with T_c being the duration of the clock cycle.

Fig. 1 gives a clear graphic illustration of the Dick effect and of the role of the dead time. The figure shows numerically generated noise around the cycle frequency $f_c = 1/T_c$ with a bandwidth of $0.3\,f_c$. The noise of the oscillator enters in the clock measurement as the time average of $\delta\omega(t)$ weighted by $g(t)$, according to (1). For large dead times (squares in Fig. 1) only the maxima of the relevant noise components contribute to the measurement, resulting in a large dispersion of the measured frequency. When the duty cycle d approaches 1, the sensitivity function comprises almost the totality of each cycle, and the frequency fluctuations of the interrogation oscillator are averaged out. This averaging effect is almost perfect in the case of Ramsey interaction (stars in Fig. 1 for $d = 0.94$) since the sensitivity function is a constant during the free evolution period. As T_d approaches 0, the measurement noise totally vanishes provided the interrogation pulses are kept short enough ($\tau_p \ll T_d$). The situation is quite different for Rabi interrogation (circles in Fig. 1), since the sinusoidal shape of $g(t)$ enfeebles the efficiency of the averaging process. The averaging effect and the different behavior depending on the interrogation scheme is further illustrated in Fig. 2, where the Allan deviation as a function of the duty cycle is

978-1-4244-3510-4/09/$25.00 ©2009 IEEE

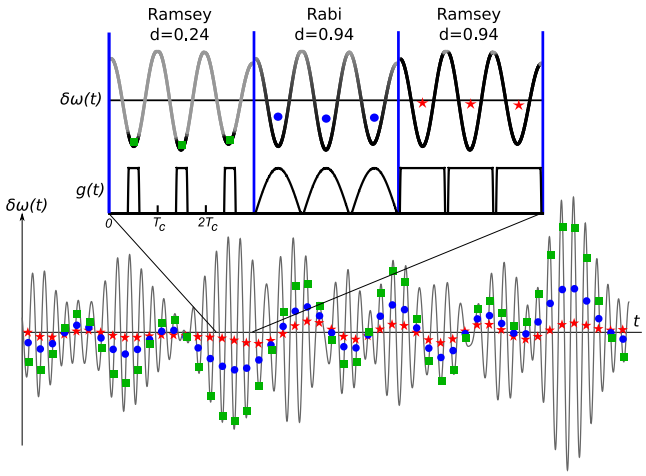

Fig. 1. Simulated frequency noise $\delta\omega(t)$ of the interrogation oscillator filtered around the cycle frequency $f_c = 1/T_c$ with a bandwidth of $0.3\,f_c$. The points show the weighted average $\int g(t)\delta\omega(t)dt/\int g(t)dt$ for Rabi interrogation with duty cycle $d = 0.94$ (circles) and for Ramsey interrogation with duty cycles $d = 0.24$ (squares) and $d = 0.94$ (stars). The inset shows how $\delta\omega(t)$ is sampled over 3 cycles for the three different sensitivity functions $g(t)$.

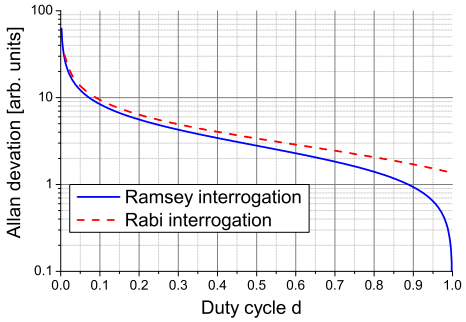

Fig. 2. Dick limited Allan deviation $\sigma_y(\tau)$ for white frequency noise for a given τ for Rabi and Ramsey interrogation. In the case of Ramsey interaction, the Dick effect vanishes for $d \to 1$ if τ_p is kept smaller than T_d. The curves are computed using (2).

plotted [1]. Due to this clear advantage of Ramsey interrogation, we restrict further analysis to this case only.

The limitation of the fractional Allan variance due to the interrogation laser frequency noise is given by [8]

$$\sigma_y^2(\tau) = \frac{1}{\tau g_0^2} \sum_{m=1}^{\infty} |g_m|^2 \, S_y(m/T_c), \qquad (2)$$

where $S_y(f)$ is the one-sided power spectral density of the relative frequency fluctuations of the free running interrogation oscillator taken at Fourier frequencies m/T_c. The Fourier coefficients of $g(t)$ are given by

$$g_m = \frac{1}{T_c} \int_0^{T_c} g(t) e^{-2\pi i m t/T_c} dt. \qquad (3)$$

[1] We chose to plot Fig. 2 in the case where the interrogation laser exhibits white frequency noise. This is the only type of noise where the Allan deviation only depends on the duty cycle, and not on the specific parameters chosen.

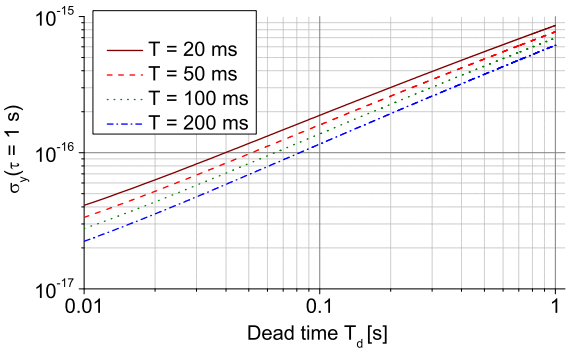

Fig. 3. Fractional Allan deviation $\sigma_y(\tau = 1\,\mathrm{s})$ *vs* dead time for various durations of the Ramsey interrogation T. The duty cycle is $d = 0.02$ for $T_d = 1.0\,\mathrm{s}$ and $T = 0.02\,\mathrm{s}$, and $d = 0.95$ for $T_d = 0.01\,\mathrm{s}$ and $T = 0.2\,\mathrm{s}$.

State-of-the-art interrogation laser stabilization is performed by locking the laser frequency to an ultra-stable Fabry-Perot cavity. In the following, we assume that the dominant source of noise is the thermal noise of the cavity $S_y(f) = h_{-1} f^{-1}/\nu^2$ with ν being the clock frequency ($\nu = 4.29 \cdot 10^{14}\,\mathrm{Hz}$ for a Sr lattice clock). We take $h_{-1} = 4 \cdot 10^{-2}$ Hz^4 which is a worst case estimate for the ULE cavity with fused silica mirrors described in [14]. It corresponds to a constant Allan standard deviation of $6 \cdot 10^{-16}$.

Figure 3 displays the Allan deviation computed numerically using (2) as a function of dead time T_d for various T. We choose $\tau_p = 5\,\mathrm{ms}$ which is significantly shorter than the shortest T_d considered here and still long enough to keep the τ_p dependent frequency shifts (light shift, line pulling by other atomic resonances, etc...) reasonably small. Fig. 3 is another illustration of the averaging process discussed above. In present optical lattice clocks, the dead time is on the order of 1 s and the limitation of the clock stability due to the Dick effect is close to 10^{-15} [2]. Reducing this dead time down to 10 ms would improve the clock stability by almost two orders of magnitude. This consideration motivated the development of the non-destructive detection scheme which is presented in the next section. Note also that for a given dead time, it is desirable to lengthen as much as possible the Ramsey interaction. This is true as long as the linear model giving (2) holds, *i.e.* as long as the interrogation laser frequency fluctuations remain much smaller than the width of the Ramsey fringes. With the level of noise chosen for plotting Fig. 3 - that is, frequency fluctuations of the interrogation oscillator on the order of 0.3 Hz - the model therefore holds for Ramsey times up to about 200 ms.

III. Non-Destructive Measurement

We briefly recall here the main features of the scheme which allows optimization of the clock stability as discussed

[2] Measured Allan deviations are somehow higher than the value calculated here. This results mainly from the fact that the interrogation lasers used for these experiments are referenced to cavities with ULE mirror substrates, which exhibit substantially higher thermal noise than the cavities considered here.

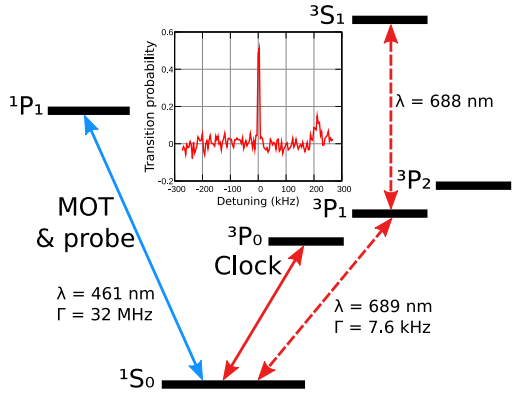

Fig. 4. Energy levels of Sr of interest here. The inset shows a typical spectrum of the clock transition using the non-destrucitve detection.

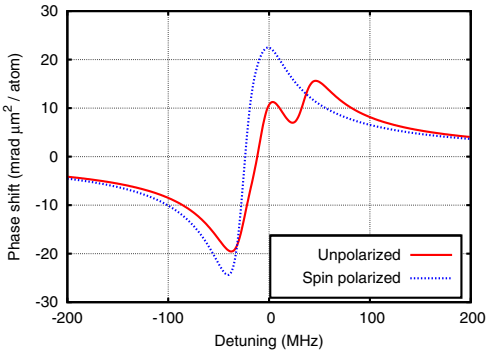

Fig. 5. Theoretical phase shift $\varphi^{at} S/N$ for the $^1S_0 - {}^1P_1$ transition with zero magnetic field and a linearly polarized probe. It takes into account the three different $F' = 7/2,\ 9/2$ and $11/2$ levels of $^1P_1$, spanning over 60 MHz around their average frequency (center of the plot). The phase shift is represented for equally populated m_F states (solid red curve) and spin-polarized atoms in $m_F = 9/2$ or $m_F = -9/2$ states (dashed blue curve). For a 90 MHz detuning, these phase shifts are comparable and amount to a few tens of mrad with typical parameters $N = 10^4$ atoms and $S = 2.8 \cdot 10^3 \mu\text{m}^2$.

in section IV. More details can be found in [16].

A. Theoretical Discussion

The scheme is based on the measurement of the phase shift accumulated by a weak probe beam when passing through the atomic cloud. A method using the same physical effect was demonstrated with Cs atoms in [17], [18]. For an atomic gas with states $|J, F, m_F\rangle$ and $|J', F', m'_F\rangle$, light with polarization state q and wavelength λ detuned by $\Delta_{F,F'}$ from the transition between the two states will experience a phase shift

$$\varphi^{at} = \frac{3\lambda^2(2J'+1)}{4\pi S} \sum_{F,m_F,F',m'_F} N_{m_F}(2F'+1)(2F+1) \qquad (4)$$
$$\times \underbrace{\begin{pmatrix} F' & 1 & F \\ m'_F & q & -m_F \end{pmatrix}^2}_{\text{Wigner } 3j \text{ symbol}} \underbrace{\begin{Bmatrix} J & J' & 1 \\ F' & F & I \end{Bmatrix}^2}_{\text{Wigner } 6j \text{ symbol}} \frac{(\Gamma/2)\Delta_{F,F'}}{\Delta^2_{F,F'} + (\Gamma/2)^2}$$

where N_{m_F} is the atomic population in the hyper-fine substate $|F, m_F\rangle$, Γ is the natural linewidth of the transition and S is the cross-section of the atomic cloud. With a Gaussian distributed laser beam and atomic cloud, averaging the phase shift over the transverse directions gives $S = 2\pi(r_0^2 + w^2/4)$ where r_0 is the cloud standard deviation and w the $1/e^2$ radius of the laser beam.

(4) shows that if $|J, F, m_F\rangle$ is one of the two clock states, φ^{at} gives a measure of the number of atoms that populate this state after the clock interrogation, yielding the clock transition probability. We have chosen to operate with the $^1S_0 - {}^1P_1$ transition, for which the induced phase shift is plotted in Fig. 5.

B. Experimental Setup

The phase shift measurement setup uses an electro-optic phase modulator (EOM) in a Mach-Zender (MZ) interferometer (Fig. 6). A laser beam resonant with the $^1S_0 - {}^1P_1$ transition is split into a weak signal (typically a few nW) and a strong local oscillator (LO) (a few mW). The signal beam is modulated at 90 MHz by the EOM before it is overlapped with the atoms in the optical lattice. The signal beam waist is $w = 37\ \mu$m, comparable to the transverse size of the

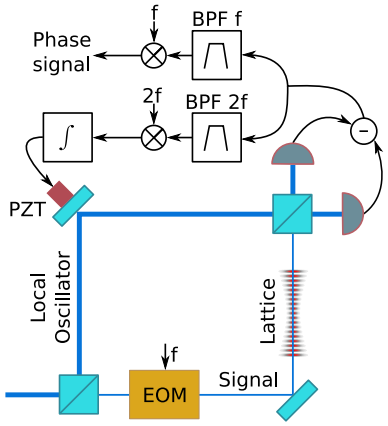

Fig. 6. Experimental setup. The number of atoms in the optical lattice is proportionnal to the phase shift of the RF component at the modulation frequency f, filtered by a band-pass filter (BPF). The harmonic at frequency $2f$ is used to lock the phase of the interferometer, hence maximizing the RF power of the signal component.

atomic ensemble ($r_0 = 10\ \mu$m). The electric field of the signal beam is detected by a homodyne detection in which the signal interferes with the LO on a beam splitter and the light intensities in each output arm of the beam splitter are measured with fast Si photodiodes (Hamamatsu S5973) and electrically subtracted. In this scheme, the LO amplifies the signal without degrading its signal to noise ratio (SNR) [19]. For a LO power of 2 mW the electronic noise is smaller than the photon shot noise by a factor of 2.

The RF output s of the difference of the photocurrents is (up to a constant factor):

$$s = \sum_{n=1}^{+\infty} J_n(a) h\left(\phi_0 - \frac{\varphi_n + \varphi_{-n}}{2}\right) h\left(n\omega t + \frac{\varphi_n - \varphi_{-n}}{2}\right) \qquad (5)$$

where J_n is the Bessel function of the first kind, ϕ_0 the phase of the LO, a the modulation depth, ω the modulation angular frequency and $h = \cos$ (sin) if n is even (odd). φ_n is the total

phase shift experienced by the modulation sideband n. It can be expanded as $\varphi_n = \varphi^{at}(n\omega) + \delta\varphi_n + \phi_s$ where $\varphi^{at}(n\omega)$ is the atomic phase shift for a detuning $n\omega$ given by equation (4), ϕ_s is a global phase and $\delta\varphi_n$ is the laser phase noise. Because all the modulation sidebands belong to the same spatial mode, ϕ_s is independent of n. Given the low power at which we operate and the small line-width of our laser (< 1 MHz), $\delta\varphi_n$ is dominated by shot noise, even though our interferometer features an optical path difference of about 2 m between the signal and the LO.

We can see from (5) that the phase of the RF component at angular frequency $n\omega$ is the differential atomic phase shift of the $-n$ and $+n$ modulation sidebands. Since φ^{at} is approximately an odd function of the probe detuning, this phase shift is proportional to the number of atoms in the atomic ground state. Furthermore, it does not depend on the phase ϕ_0 of the LO nor the global phase ϕ_s of the signal, making our system independent of mechanical and thermal fluctuations. These features are very welcome given the small phase shifts we want to detect. However, the amplitude of the RF components does depend on ϕ_0, and will eventually cross zero as ϕ_0 drifts. The parity of h shows in particular that the odd RF sidebands have maximum power when the amplitude of the even sidebands is null. We use this feature to lock ϕ_0: we demodulate the second order RF component at angular frequency $2\,\omega$ and servo-loop ϕ_0 with a piezoelectric transducer (PZT) to keep the demodulation signal at zero. The lock bandwidth is 10 kHz, limited by the mechanical properties of the PZT. Finally, the atomic phase signal is extracted by demodulating the first order RF component, maximized by the lock (Fig. 6). We emphasize that the noise of this phase signal does not depend on the noise of the PZT lock to first order, due to the quadrature detection.

C. Modulation Parameters

We choose the modulation frequency $f = \omega/2\pi$ and amplitude a to optimize the signal to noise ratio (SNR) of the detection scheme. The final SNR results from a trade-off between the phase component of the optical shot noise which decreases at larger optical powers, and the heating of the atomic cloud which increases with the optical power as long as the transition is not saturated. Therefore we have to determine the optimal f and a for a given heating of the atoms. The signal to noise ratio is

$$SNR = \frac{\varphi^{at}(+\omega) - \varphi^{at}(-\omega)}{\sqrt{\langle\delta\varphi_1^2\rangle + \langle\delta\varphi_{-1}^2\rangle}} \quad (6)$$

$$\text{with} \quad \langle\delta\varphi_{+1}^2\rangle = \langle\delta\varphi_{-1}^2\rangle = \frac{hc}{4\lambda|J_1(a)|^2\eta P\tau_{nd}} \quad (7)$$

where P is the total optical power seen by the atoms, τ_{nd} is the detection probe time and η the detection efficiency. The product $P\tau_{nd}$ is linked to the number of photons n_γ absorbed by each atom of the atomic ensemble, characterizing the fraction of the atoms lost during the non-destructive probing,

$$n_\gamma = P\tau_{nd}\frac{\Gamma}{2P_{sat}}\sum_{n=-\infty}^{+\infty}\frac{|J_n(a)|^2}{1+4(n\omega)^2/\Gamma^2}. \quad (8)$$

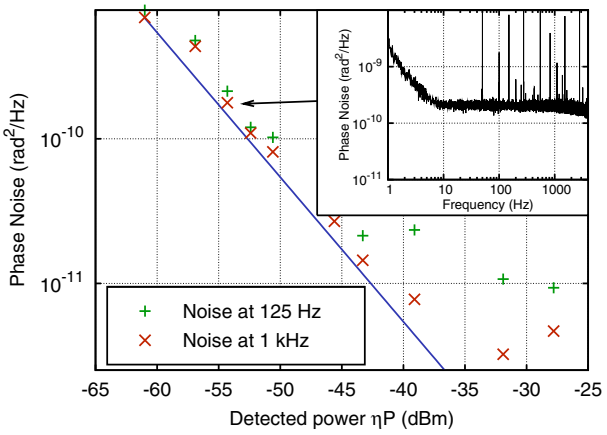

Fig. 7. Detection noise ($\frac{1}{2}\sqrt{\langle\delta\varphi_1^2\rangle + \langle\delta\varphi_{-1}^2\rangle}$) power spectral density at 125 Hz and 1 kHz. The signal is shot noise limited (blue line, from (7)) for powers up to 30 nW. The inset shows the full phase noise spectrum for a typical detected optical power $\eta P = 3$ nW, corresponding to a white noise level of 2×10^{-10} rad^2/Hz.

Here, $P_{sat} = 1.2\ \mu$W is the saturation power averaged over the atomic cloud. Combining equations (6-8) gives an expression of the SNR as a function of ω and a. We find that the SNR increases with ω and saturates after a few Γ. In our experimental setup, we have chosen $\omega = 2\pi\,90$ MHz $\simeq 3\Gamma$ for which the SNR is nearly optimal. For this frequency, the optimal a computed from equations (6-8) is very close to the modulation amplitude for which the resonant carrier is completely suppressed ($a = 2.4$ rad). Furthermore, the SNR is very flat around this optimum so that temperature control of the EOM is not required. For $a = 2.4$ rad, the $+1$ and -1 modulation sidebands have 53% of the optical power. The remaining power distributed in the higher order sidebands contributes to the heating of the atoms but not to the signal. From the previous equations, we calculate that these higher order sidebands degrade the SNR by 8 % only.

Finally, the contrast of our interferometer is 76% (measured with a balanced MZ configuration) and 25% additional optical losses appear between the atoms and the detection. These defects are attributed to the vacuum chamber windows and the optics of the lattice cavity that were not originally designed to operate at the probe wavelength. As a result the detection efficiency is $\eta = 43\%$.

D. Detection Noise

1) Detectivity: We characterize the noise of the measurement setup as follows. A typical noise spectrum of the phase signal is shown in Fig. 7. It is shot noise limited from 10 Hz. The detection system features a noise floor at 10^{-11} rad^2/Hz, so that the signal is shot noise limited for total optical powers up to 30 nW. Given this noise figure, we probe the atoms with $\tau_{nd} = 3$ ms signal pulses of typically $P = 12$ nW ($\eta P = 5$ nW). These pulses have a product $P\tau_{nd}$ low enough to keep most of the atoms in the lattice (see section III-E). They are short enough to escape the low frequency noise, and long compared to the PZT lock bandwidth.

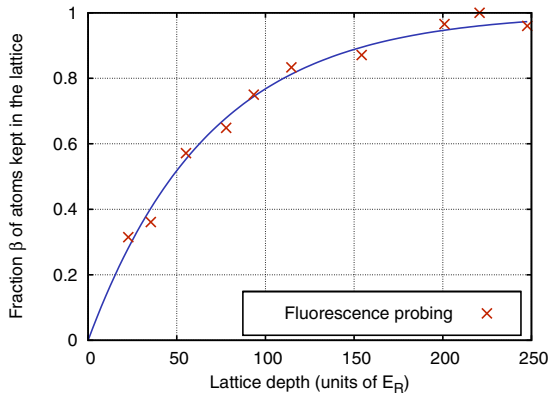

Fig. 8. Atomic loss due to the detection probe for different lattice depths, measured by fluorescence detection after the non-destructive probing. The solid curve is a fit of the fluorescence points with (9). This fit gives n_γ = 103 photons per atom, in good agreement with the value of 81 photons per atom deduced from (8) and the measured optical power ($P = 14$ nW, $\tau_{nd} = 3$ ms).

To measure the atomic population in $^1S_0$, we apply two consecutive probe pulses separated by a 7 ms interval. Between these pulses we shelve the atoms in the the dark states $^3P_0$ and $^3P_2$ by optical pumping on the $^1S_0 - {}^3P_1$ and $^3P_1 - {}^3S_1$ transitions. The second probe pulse does not experience the atomic phase shift and then acts as a zero phase reference. During the probe pulses, the phase signal is sampled at 500 kHz and the final signal is the difference of the averaged signal over each the probe duration. The noise of the resulting signal, as measured with no atoms in the lattice, is 0.4 mrad RMS for $\eta P = 5$ nW and scales as $1/\sqrt{P}$ as expected from equation (6).

With about $N = 10^4$ atoms in the lattice, we measured a phase shift of 40 mrad corresponding to a SNR of 100 per cycle, which is close to the expected atomic quantum projection noise.

2) Transition Probability: The measurement of the absolute transition probability associated with the interrogation of the atomic ensemble with our clock laser involves a third probe pulse. All probe pulses should be applied after the clock interrogation since low frequency phase drifts would add noise to the detection signal for long interrogation times. The sequence is as follows: after the clock interrogation a first probe pulse measures the number of atoms that remained in the atomic ground state. Then the atoms are repumped into the fundamental state, and are probed with a second probe pulse that determines the total number of atoms. Then, as before, we pump all the atoms into the dark states and apply a reference pulse. The measured noise on the transition probability is $\sigma_{\delta P} = 2\%$ RMS with the previous parameters, and varies as $1/N$ for N up to 10^4.

E. Heating

A key feature of the detection scheme is the ability to recycle the atoms from one cycle to the other. To check that the detection pulses do not heat the atoms out of the lattice, we measured the atomic losses caused by the phase detection with a fluorescence probe at the end of each clock cycle. This measurement has been repeated for different lattice depths (Fig. 8). We model the heating process by absorption and spontaneous emission. Because the detection probe beam is aligned with the lattice axis and the atoms are in the Lamb-Dicke regime in this direction, we assume that the recoil momentum associated with photon absorption is absorbed by the lattice and does not contribute to heating the atoms. However, the trapping potential is loose in the transverse directions, and therefore the horizontal component of the recoil momentum associated with spontaneous emission is entirely transferred to the atoms. For atoms initially in the vibrational ground state of the lattice, the fraction β of atoms remaining in the lattice after detection is:

$$\beta = 1 - \exp\left(-\frac{U_0/E_R}{2n_\gamma/3}\right) \tag{9}$$

where U_0 is the lattice depth, $E_R = \frac{h^2}{2m\lambda^2}$ is the recoil energy associated with the interaction between a Sr atom with mass m and a probe photon ($\lambda = 461$ nm), and n_γ is the number of absorbed photons per atom, given by (8). As shown in Fig. 8, this model is in agreement with the experiment. We observed that for a lattice depth around 200 E_R, more than 95% of the atoms remain trapped after the detection pulses. This important depth does not hamper the clock accuracy since the lattice depth can ramped down to a few E_R during the clock interrogation.

IV. Optimization of the Strontium Clock Time Sequence

The time sequence for operation of the Sr lattice clock is sketched in Fig. 9. The dead time T_d can be split up into two components, $T_d = T_M + \widetilde{T}_d$, where T_M is the capture time for the atoms, and $\widetilde{T}_d$ is the time used for cooling, optical pumping, and detection of the atoms. The present minimum residual dead time of the sequence is $\widetilde{T}_d = 70$ ms, mainly limited by the duration of the narrow line cooling in the lattice referred to as "Red cooling" on the figure. The duration of this cooling was adjusted so as to optimize the atomic temperature in the lattice at a fixed laser frequency and power. By allowing a variation of these parameters the duration could certainly be shortened significantly. However, to give a conservative estimate of the optimized clock stability we keep this duration at its present value. The two parameters left for optimization are therefore the duration of the capture phase ("MOT+Drain" on Fig. 9) T_M and the Ramsey interrogation time T.

The optimal time sequence results from a balance between the Dick effect and the detection noise. Taking both into account, the Allan variance of the clock is given by

$$\sigma^2_{\text{tot}}(\tau) \quad = \quad \sigma^2_y(\tau) + \sigma^2_{\text{det}}(\tau), \tag{10}$$

where σ_y is defined in section II and σ_{det} is given by

$$\sigma_{\text{det}}(\tau) = \left(\frac{2}{\pi Q}\right)\sigma_{\delta P}\sqrt{\frac{T_c}{\tau}}, \tag{11}$$

Q and $\sigma_{\delta P}$ being the atomic quality factor and the standard deviation of the detected transition probability. $\sigma_{\delta P}$ scales as

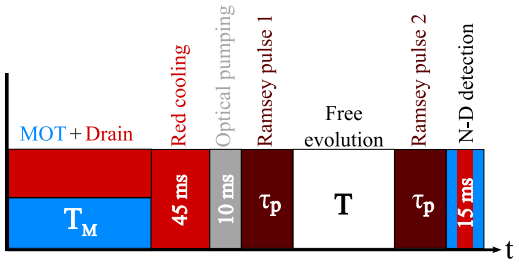

Fig. 9. The time sequence for the Sr lattice clock. For further details, see [20]. The minimum residual dead time $\widetilde{T}_d = T_d - T_M$ of this sequence is 70 ms.

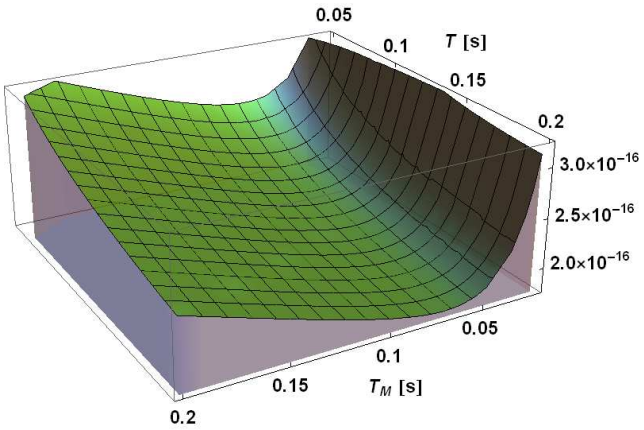

Fig. 10. The total fractional Allan deviation at 1 s as a function of capturing time T_M and Ramsey dark time T with residual dead time $\widetilde{T}_d = 70$ ms.

the inverse of the atom number N up to $N = 10^4$ for which $\sigma_{\delta P} = 0.02$ as shown in section III-D.

The non-destructive detection scheme allows recycling of the atoms, so that the number of atoms in cycle j is given by

$$\begin{aligned} N_j &= N_L + \xi N_{j-1} e^{-T_c/\tau_t}, \\ N_L &= N_{\max}(1 - e^{-T_M/\tau_t}) e^{-(T_c - T_M)/\tau_t}, \end{aligned} \tag{12}$$

where N_L is the number of atoms loaded into the trap in each cycle, τ_t is the lifetime of the cold atoms in the lattice, and $N_{\max}$ is, for a given τ_t, the maximally achievable number of atoms in the trap, that is for $T_M \to \infty$. ξ is the fraction of atoms kept in the trap between cycles. For our experiment, $N_{\max} = \tau_t \cdot 1.8 \cdot 10^4$/s, $\tau_t = 1.5$ s and $\xi = 0.95$.

From (12) we get the steady-state number of atoms

$$N = N_{\max} \frac{e^{T_M/\tau_t} - 1}{e^{T_c/\tau_t} - \xi}. \tag{13}$$

Fig. 10 displays $\sigma_{\text{tot}}(1\,\text{s})$ as a function of both T_M and T. To remain in the validity domain of the model, we limited the range of variation of T up to 200 ms as for Fig. 3. Once again, the optimal T is the longest allowed one, $T = 200$ ms. The corresponding optimal value for the loading time is $T_M = 69$ ms giving $\sigma_{\text{tot}}(\tau) = 1.8{\cdot}10^{-16}\,\tau^{-1/2}$. The individual contributions of the Dick effect and of the detection noise are $\sigma_y(\tau) = 1.5 \cdot 10^{-16}\,\tau^{-1/2}$ and $\sigma_{\text{det}}(\tau) = 1.0 \cdot 10^{-16}\,\tau^{-1/2}$,

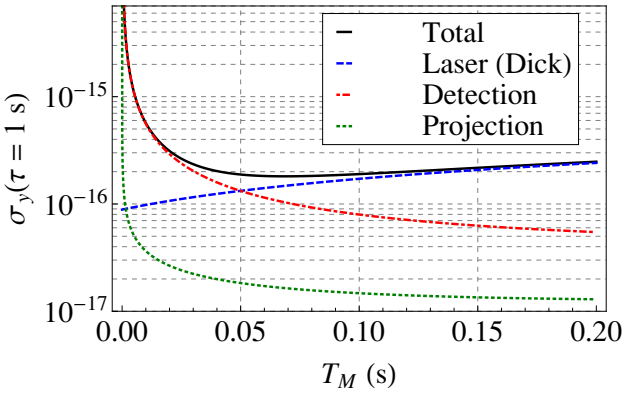

Fig. 11. The different contributions to the total fractional Allan deviation at 1 s as a function of capturing time T_M for Ramsey dark time $T = 200$ ms with residual dead time $\widetilde{T}_d = 70$ ms.

respectively. Finally, the steady-state number of atoms in the optimized configuration is $N = 4000$.

The individual contributions to $\sigma_{\text{tot}}(\tau = 1\,\text{s})$ for $T = 200$ ms are shown in Fig. 11. The contribution from the quantum projection noise also is included in the plot, showing that σ_{tot} is still well above the quantum limit, leaving room for further improvements. These improvements would include increasing the trap lifetime and reducing the residual dead time as well as enhancing the coherence time of the interrogation laser.

V. Conclusion

We have shown that in parallel to the reduction of the interrogation laser frequency noise, the optimization of the time sequence could be a very efficient way to minimize the Dick effect in optical lattice clocks. By using a non-destructive detection scheme together with an adapted time sequence, the Allan deviation of our clock could be optimized down to below $2 \cdot 10^{-16}\,\tau^{-1/2}$, which would outperform current state-of-the-art by about one order of magnitude.

Though very encouraging, this result is still about one order of magnitude above the expected quantum limit of the clock. In the optimized time sequence presented in section IV the duty cycle is "only" 0.60 and large room for improvement remains. Cooling the atoms down to their minimal temperature presently takes 45 ms which could probably be strongly reduced by using a more sophisticated time sequence, for instance allowing both the frequency and power of the cooling laser to vary during this phase. On the other hand, the lifetime of the atoms in the lattice is presently limited to 1.5 s, so that about 20 % of the atoms need to be reloaded at each cycle. This leads to a relatively long loading time of 69 ms in the optimized configuration. We have not yet investigated in detail the limiting factors of this lifetime in our setup but we see no fundamental reasons preventing atoms from being kept in the lattice for ten seconds or more. With such a lifetime, one would take full advantage of the non-destructive detection scheme described in section III, giving a $\sigma_{\text{tot}}(\tau = 1\,\text{s})$ on the order of $1 \cdot 10^{-16}$.

SYRTE is a member of IFRAF (Institut Francilien de Recherche sur les Atomes Froids). This work has received funding from the European Community's Seventh Framework Programme, ERA-NET Plus, under Grant Agreement No. 217257, as well as from IFRAF, CNES and ESA.

REFERENCES

[1] H. Katori, M. Takamoto, V. G. Pal'chikov, and V. D. Ovsiannikov, "Ultrastable optical clock with neutral atoms in an engineered light shift trap," *Phys. Rev. Lett.*, vol. 91, p. 173005, 2003.

[2] M. M. Boyd, T. Zelevinsky, A. D. Ludlow, S. M. Foreman, S. Blatt, T. Ido, and J. Ye, "Optical atomic coherence at the 1-second time scale," *Science*, vol. 314, no. 5804, pp. 1430–1433, 2006.

[3] F.-L. Hong, M. Musha, M. Takamoto, H. Inaba, S. Yanagimachi, A. Takamizawa, K. Watabe, T. Ikegami, M. Imae, Y. Fujii, M. Amemiya, K. Nakagawa, K. Ueda, and H. Katori, "Measuring the frequency of a Sr optical lattice clock using a 120-km coherent optical transfer," *arXiv:0811.1816*, 2008.

[4] X. Baillard, M. Fouché, R. Le Targat, P. G. Westergaard, A. Lecallier, F. Chapelet, M. Abgrall, G. D. Rovera, P. Laurent, P. Rosenbusch, S. Bize, G. Santarelli, A. Clairon, P. Lemonde, G. Grosche, B. Lipphardt, and H. Schnatz, "An optical lattice clock with spin-polarized ^{87}Sr atoms," *EPJD*, vol. 48, no. 1, p. 11, 2008.

[5] A. D. Ludlow, T. Zelevinsky, G. K. Campbell, S. Blatt, M. M. Boyd, M. H. G. de Miranda, M. J. Martin, J. W. Thomsen, S. M. Foreman, J. Ye, T. M. Fortier, J. E. Stalnaker, S. A. Diddams, Y. L. Coq, Z. W. Barber, N. Poli, N. D. Lemke, K. M. Beck, and C. W. Oates, "Sr lattice clock at 1×10^{16} fractional uncertainty by remote optical evaluation with a Ca clock," *Science*, vol. 319, pp. 1805–1808, 2008.

[6] Z. W. Barber, J. E. Stalnaker, N. D. Lemke, N. Poli, C. W. Oates, T. M. Fortier, S. A. Diddams, L. Hollberg, C. W. Hoyt, A. V. Taichenachev, and V. I. Yudin, "Optical lattice induced light shifts in an Yb atomic clock," *Phys. Rev. Lett.*, vol. 100, no. 10, p. 103002, 2008. [Online]. Available: http://link.aps.org/abstract/PRL/v100/e103002

[7] G. Dick, "Local oscillator induced instabilities in trapped ion frequency standards," in *Proc. of Precise Time and Time Interval*, Redendo Beach, 1987, pp. 133–147.

[8] G. Santarelli, C. Audoin, A. Makdissi, P. Laurent, G. J. Dick, and A. Clairon, "Frequency stability degradation of an oscillator slaved to a periodically interrogated atomic resonator," *IEEE Trans. Ultrason., Ferroelect., Freq. Contr.*, vol. 45, pp. 887–894, 1998.

[9] A. Quessada, R. P. Kovacich, I. Courtillot, A. Clairon, G. Santarelli, and P. Lemonde, "The Dick effect for an optical frequency standard," *J. Opt. B : Quantum Semiclassical Opt.*, vol. 5, p. S150, 2003.

[10] B. Young, F. Cruz, W. Itano, and J. C. Bergquist, "Visible lasers with subhertz linewidths," *Phys. Rev. Lett.*, vol. 82, pp. 3799–3802, 1999.

[11] T. Nazarova, F. Riehle, and U. Sterr, "Vibration-insensitive reference cavity for an ultra-narrow-linewidth laser," *Appl. Phys. B*, vol. 83, pp. 531–536, 2006. [Online]. Available: http://dx.doi.org/10.1007/s00340-006-2225-y

[12] A. D. Ludlow, X. Huang, M. Notcutt, T. Zanon-Willette, S. M. Foreman, M. M. Boyd, S. Blatt, and J. Ye, "Compact, thermal-noise-limited optical cavity for diode laser stabilization at 11015," *Opt. Lett.*, vol. 32, no. 6, pp. 641–643, 2007.

[13] S. A. Webster, M. Oxborrow, and P. Gill, "Vibration insensitive optical cavity," *Phys. Rev. A*, vol. 75, no. 1, p. 011801, 2007. [Online]. Available: http://link.aps.org/abstract/PRA/v75/e011801

[14] J. Millo, D. V. Magalhaes, C. Mandache, Y. L. Coq, E. M. L. English, P. G. Westergaard, J. Lodewyck, S. Bize, P. Lemonde, and G. Santarelli, "Ultrastable lasers based on vibration insensitive cavities," *Physical Review A (Atomic, Molecular, and Optical Physics)*, vol. 79, no. 5, p. 053829, 2009.

[15] K. Numata, A. Kemery, and J. Camp, "Thermal-noise limit in the frequency stabilization of lasers with rigid cavities," *Physical Review Letters*, vol. 93, no. 25, p. 250602, 2004. [Online]. Available: http://link.aps.org/abstract/PRL/v93/e250602

[16] J. Lodewyck, P. G. Westergaard, and P. Lemonde, "Non-destructive measurement of the transition probability in a Sr optical lattice clock," *arXiv:0902.2905*, 2009.

[17] D. Oblak, P. G. Petrov, C. L. Garrido Alzar, W. Tittel, A. K. Vershovski, J. K. Mikkelsen, J. L. Sørensen, and E. S. Polzik, "Quantum-noise-limited interferometric measurement of atomic noise: Towards spin squeezing on the cs clock transition," *Phys. Rev. A*, vol. 71, no. 4, p. 043807, Apr 2005.

[18] P. J. Windpassinger, D. Oblak, P. G. Petrov, M. Kubasik, M. Saffman, C. L. G. Alzar, J. Appel, J. H. Muller, N. Kjaergaard, and E. S. Polzik, "Nondestructive probing of rabi oscillations on the cesium clock transition near the standard quantum limit," *Phys. Rev. Lett.*, vol. 100, no. 10, p. 103601, 2008. [Online]. Available: http://link.aps.org/abstract/PRL/v100/e103601

[19] U. Leonhardt, *Measuring the Quantum State of Light*. Cambridge: University Press, 1997.

[20] R. L. Targat, X. Baillard, M. Fouché, A. Brusch, O. Tcherbakoff, G. D. Rovera, and P. Lemonde, "Accurate optical lattice clock with ^{87}Sr atoms," *Physical Review Letters*, vol. 97, no. 13, p. 130801, 2006. [Online]. Available: http://link.aps.org/abstract/PRL/v97/e130801